A New Phase Linking Algorithm for Multi-temporal InSAR based on the Maximum Likelihood Estimator

Phan Viet Hoa VU, Frédéric Brigui, Arnaud Breloy, Yajing Yan, Guillaume Ginolhac

HAL Id: hal-03761316

https://hal.science/hal-03761316

Submitted on 26 Aug 2022

A New Phase Linking Algorithm for Multi-temporal InSAR based on the Maximum Likelihood Estimator

Phan Viet Hoa VU[1,3], *Frédéric BRIGUI*[1], *Arnaud BRELOY*[2], *Yajing YAN*[3], and *Guillaume GINOLHAC*[3]

[1]DEMR, ONERA, Université Paris Saclay, F-91123 Palaiseau, France
[2]Paris Nanterre University, LEME EA-4416, 92410 Ville d'Avray, France
[3]Université Savoie Mont Blanc, LISTIC, F-74000 Annecy, France

ABSTRACT

This paper presents a new algorithm for improving the estimation of interferometric SAR (InSAR) phases in the context of time series and phase linking approach. Based on maximum likelihood estimator of a multivariate Gaussian model, the estimation of the InSAR phases is solved using a Block Coordinate Descent algorithm. Compared to the state-of-the-art approaches, the main improvement lies on the joint estimation of the covariance matrix and the InSAR phases instead of using a plug-in coherence estimate obtained from the sample covariance of the data or the modeling of the temporal decorrelation of the target under observation. Results of synthetic simulations confirm the improvement brought by the proposed estimator.

Index Terms— Multi-temporal InSAR, Surface Displacement Monitoring, Phase Linking, Maximum Likelihood Estimator, Block Coordinate Descent algorithm

1. INTRODUCTION

Since the last decade, the research community has been paying more attention to multi-temporal InSAR techniques, as satellite SAR images allow for the monitoring of large deforming areas with sub-centimeters accuracy [1, 2]. Recently, with the systematic acquisitions of Sentinel-1 A/B images, regular and operational monitoring of displacement with multi-temporal InSAR approaches constitutes a prevalent subject in numerous studies.

Multi-temporal InSAR approaches have been developed based on how the signal decorrelation over time can be accounted for. For this, analysing the backscattering properties of SAR images is needed to define different scatterers. In the literature, two kinds of scatterers, Permanent Scatterer (PS) and Distributed Scatterer (DS) are distinguished. The current state-of-the-art multi-temporal InSAR approaches rely on 1) processing with point-wise time coherent PS, namely PS Interferometry [3], 2) the construction of redundant interferogram networks in DS Interferometry [4]; 3) the combination

of PSI and DSI [5]. PSI approaches have widely been deployed for urban area monitoring, but its application to natural areas is often limited due to the weak PS points density. In DSI, Small BAseline Subset (SBAS) approaches use only small temporal and spatial baselines SAR image pairs in the interferogram network, with the objective to minimize signal decorrelation. With these strategies, phase bias has been observed in the displacement estimation in case of long time series [6]. Another important DSI approach corresponds to the Phase Linking (PL) approach. The main idea of this approach is to use all the $N \times (N-1)/2$ interferograms generated from a time series of N SAR images to yield the best estimate of $N-1$ single referenced phase difference [7]. This approach allows for a full exploitation of all possible combinations of a SAR image stack by formally taking the impact of the temporal decorrelation into account. Most recent advances in multi-temporal InSAR, e.g. EMI [8] and sequential estimator [9], have been developed from this baseline approach.

The Maximum Likelihood Estimator (MLE) based PL approaches (namely MLE-PL for the sake of brevity) present a statistically optimal estimator for the parameters of interest (e.g. DEM error, displacement rate). Besides properly weighting in a ML sense all the interferograms to limit spatial and temporal decorrelation, another advantage of MLE-PL approaches is that the estimates are asymptotically unbiased with a minimum variance by virtue of the properties of the MLE. In general, the MLE-PL approaches require prior and reliable information on the coherence to drive the estimation algorithm. Therefore, the performance of MLE-PL approaches strongly depends on the reliability of the prior coherence information.

In the state-of-the-art, MLE-PL approaches [7, 5, 10] do not solve the exact MLE, as they rely on a plug-in estimate of the coherence matrix. In this paper, we propose to develop the MLE-PL by jointly solving the estimation of all parameters (phases and covariance matrix). The proposed approach is based on the block coordinate descent (BCD). Additionally, we derive a Majorization-Minimization algorithm to solve the PL step. Simulations illustrate the interest of this approach.
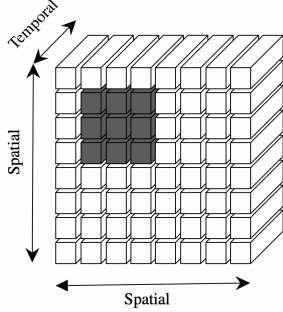
2. SAR TIME SERIES MODEL

Fig. 1. SAR time series datacube representation. Sliding window (in gray) $\mathbf{x}$ on dataset of the single-look-complex SAR acquisitions.

A time series of N SAR images are stacked along the temporal and spatial dimensions into a cube (Figure 1). Sliding window $\mathbf{x}_i$ (colored in gray) contains a local observation for N snapshots:

$$\mathbf{x}_i = [x_i^0, ..., x_i^{N-1}]^\top \qquad (1)$$

Within the scope of this study, we assume that the set $\{\mathbf{x}_i\}_{i=1}^L$ with $\mathbf{x}_i \in \mathbb{C}^N$, $\forall i \in [1, L]$ are distributed scatterers which are spatially homogeneous over L adjacent pixels. $\{\mathbf{x}_i\}_{i=1}^L$ is thus a set of independent and identically distributed (i.i.d.) vectors. As in the current literature, we assume in this paper that $\mathbf{x}_i$ follows a zero-mean complex circular Gaussian distribution with the probability density function (PDF) of

$$f(\mathbf{x}, \mathbf{C}) = \frac{1}{\pi^N \mathrm{Det}(\mathbf{C})} \exp\left(-\mathbf{x}^H \mathbf{C}^{-1}\mathbf{x}\right) \qquad (2)$$

The second moment of $\mathbf{x}$ relates to interferograms which is given $\forall (k,l) \in [0, N-1]^2$ by

$$\mathbb{E}[x^l(x^k)^*] = \gamma_{k,l}\sigma_k\sigma_l \exp(j(\theta_l - \theta_k)), \qquad (3)$$

where:

- $\sigma_n^2 = \mathbb{E}[x^n(x^n)^H]$ is the variance of x^n. The vector of standard deviation is denoted as $\boldsymbol{\sigma} = [\sigma_0, ..., \sigma_{N-1}]$

- $\gamma_{k,l} \in [-1, 1]$ is the correlation coefficient between x^k and x^l. We denote $\boldsymbol{\Gamma}$ the matrix with entries $[\boldsymbol{\Gamma}]_{k,l} = \gamma_{k,l}$. $[\boldsymbol{\Gamma}]_{l,l} = 1, \forall l \in [0, N-1]$

- θ_n is the phase of image n. $\boldsymbol{\theta} = [\theta_0, ..., \theta_{N-1}]$.

Equation 3 can be rewritten in matrix form as

$$\mathbb{E}[\mathbf{x}\mathbf{x}^H] \triangleq \mathbf{C} = \mathrm{ediag}(\boldsymbol{\theta}) \underbrace{((\boldsymbol{\sigma}\boldsymbol{\sigma}^\top) \circ \boldsymbol{\Gamma})}_{\boldsymbol{\Sigma}} \mathrm{ediag}(\boldsymbol{\theta})^H \qquad (4)$$

where $\boldsymbol{\Sigma}$ denotes the covariance matrix and with

$$\mathrm{ediag}(\boldsymbol{\theta}) = \begin{pmatrix} \exp(j\theta_0) & & \mathbf{0} \\ & \ddots & \\ \mathbf{0} & & \exp(j\theta_{N-1}) \end{pmatrix} \qquad (5)$$

The matrix $\mathbf{C}$ fully characterises the InSAR phases and coherence. The InSAR principle is then to estimate all the elements of $\mathbf{C}$. Since $\boldsymbol{\Sigma}$ is unknown in practice, several papers [7, 5, 10] considered using a plug-in estimate to solve for the MLE of $\boldsymbol{\theta}$ (assuming known $\boldsymbol{\Sigma}$). This estimate is usually $|\mathbf{S}|$, i.e., the entry-wise modulus of the the sample covariance matrix (SCM). This two-step approach yields good results in practice, however it is know to be sub-optimal in terms of MSE. We propose in this paper to jointly estimate the matrix $\mathbf{C}$ and the phase difference by solving the MLE with an iterative approach.

3. NEW PHASE LINKING BASED ON THE MAXIMUM LIKELIHOOD ESTIMATOR

We reparameterize the equation (4) as

$$\mathbf{C}(\boldsymbol{\Sigma}, \boldsymbol{\theta}) = \mathrm{ediag}(\boldsymbol{\theta})\boldsymbol{\Sigma}\,\mathrm{ediag}(\boldsymbol{\theta})^H \qquad (6)$$

The maximum likelihood estimator corresponds to the solutions of the (negative log likelihood) minimization problem

$$\begin{aligned} \underset{\boldsymbol{\Sigma}, \boldsymbol{\theta}}{\mathrm{minimize}} \quad & \mathcal{L}\left(\mathbf{C}\left(\boldsymbol{\Sigma}, \boldsymbol{\theta}\right)\right) \\ \mathrm{subject\ to} \quad & \boldsymbol{\Sigma} \text{ real symmetric} \\ & \theta_0 = 0 \end{aligned} \qquad (7)$$

where $\mathcal{L}$ is the log-likelihood associated with model (2). We propose a Block Coordinate Descent (BCD) algorithm to compute the MLE. This corresponds to an algorithm that iteratively minimizes the objective w.r.t to each variable ($\boldsymbol{\Sigma}$ or $\boldsymbol{\theta}$) while keeping the other fixed.

Update $\boldsymbol{\Sigma}$

Let us update the variable $\boldsymbol{\Sigma}$ by minimizing $\mathcal{L}$ with fixed $\boldsymbol{\theta}$. The problem becomes

$$\begin{aligned} \underset{\boldsymbol{\Sigma}}{\mathrm{minimize}} \quad & \log|\boldsymbol{\Sigma}| + \mathrm{Tr}\left\{\boldsymbol{\Sigma}^{-1}\mathrm{ediag}(\boldsymbol{\theta})^H\mathbf{S}\,\mathrm{ediag}(\boldsymbol{\theta})\right\} \\ \mathrm{subject\ to} \quad & \boldsymbol{\Sigma} \text{ real symmetric} \end{aligned}$$
$$\qquad (8)$$

where we used the two following relations

$$\begin{aligned} \mathbf{C}^{-1}\left(\boldsymbol{\Sigma}, \boldsymbol{\theta}\right) &= \left(\mathrm{ediag}(\boldsymbol{\theta})\boldsymbol{\Sigma}\mathrm{ediag}(\boldsymbol{\theta})^H\right)^{-1} \\ &= \mathrm{ediag}(\boldsymbol{\theta})\boldsymbol{\Sigma}^{-1}\mathrm{ediag}(\boldsymbol{\theta})^H \end{aligned} \qquad (9)$$

$$\log|\mathbf{C}\left(\boldsymbol{\Sigma}, \boldsymbol{\theta}\right)| = \log|\boldsymbol{\Sigma}| \qquad (10)$$

and dropped the multiplicative constant L. The minimizer is then obtained as the real part of the modified sample covariance matrix

$$\boldsymbol{\Sigma}^\star = \mathrm{real}(\mathrm{ediag}(\boldsymbol{\theta})^H\mathbf{S}\,\mathrm{ediag}(\boldsymbol{\theta})) \qquad (11)$$

Update $\boldsymbol{\theta}$

By fixing $\boldsymbol{\Sigma}$, the problem is referred to as phase-linking [7] or phase triangulation [10], which reads

$$\underset{\boldsymbol{\theta}}{\text{minimize}} \quad \text{Tr}\left\{\text{ediag}(\boldsymbol{\theta})\boldsymbol{\Sigma}^{-1}\text{ediag}(\boldsymbol{\theta})^H\mathbf{S}\right\}$$
$$\text{subject to} \quad \theta_0 = 0 \tag{12}$$

Let us denote $\mathbf{w}_{\boldsymbol{\theta}} = \left[e^{j\theta_0}, \cdots, e^{j\theta_{N-1}}\right]^T$. We then have the relation

$$\text{Tr}\left\{\text{ediag}(\boldsymbol{\theta})\boldsymbol{\Sigma}^{-1}\text{ediag}(\boldsymbol{\theta})^H\mathbf{S}\right\} = \mathbf{w}_{\boldsymbol{\theta}}^H(\boldsymbol{\Sigma}^{-1} \circ \mathbf{S})\mathbf{w}_{\boldsymbol{\theta}}. \tag{13}$$

Let us also denote the set of vector with entry-wise unit norm as

$$\mathcal{U}_N = \{\mathbf{w} \in \mathbb{C}^N \mid |[\mathbf{w}]_i| = 1, \forall i \in [\![0, N-1]\!]\}. \tag{14}$$

From these notations, we need to know how to solve the generic problem

$$\underset{\mathbf{w} \in \mathcal{U}_N}{\text{minimize}} \quad \mathbf{w}^H\mathbf{M}\mathbf{w} \tag{15}$$

that allows us to obtain a solution $\boldsymbol{\theta}^\star$ for (12) from the phases of a solution $\mathbf{w}^\star$ of (15) (when plugging $\mathbf{M} = \boldsymbol{\Sigma}^{-1} \circ \mathbf{S}$). If we restrict $\mathbf{w}$ to the constrained set $\mathcal{U}_N$, we have the relation

$$\mathbf{w}^H(\mathbf{M} - \lambda_{\max}^{\mathbf{M}}\mathbf{I})\mathbf{w} = \mathbf{w}^H\mathbf{M}\mathbf{w} - \underbrace{N\lambda_{\max}^{\mathbf{M}}}_{\text{const.}} \tag{16}$$

Hence, optimizing either the objective in (15) or (16) on $\mathcal{U}_N$ will lead to the same solution. The quadratic form $\mathbf{w}^H(\mathbf{M} - \lambda_{\max}^{\mathbf{M}}\mathbf{I})\mathbf{w}$ is concave, thus it can be majorized at point $\mathbf{w}_t$ by its first order Taylor expansion

$$g(\mathbf{w}|\mathbf{w}_t) = 2\Re\mathfrak{e}\{\mathbf{w}^H\underbrace{(\mathbf{M} - \lambda_{\max}^{\mathbf{M}}\mathbf{I})\mathbf{w}_t}_{-\tilde{\mathbf{w}}_t}\} + \text{const.} \tag{17}$$

with equality achieved at $\mathbf{w}_t$. Minimizing this surrogate corresponds to the problem

$$\underset{\mathbf{w} \in \mathcal{U}_N}{\text{maximize}} \quad 2\Re\mathfrak{e}\{\mathbf{w}^H\tilde{\mathbf{w}}_t\} \tag{18}$$

whose solution is $\mathbf{w}^\star = \mathcal{P}_{\mathcal{U}_N}\{\tilde{\mathbf{w}}_t\}$, where $\mathcal{P}_{\mathcal{U}_N}\{\cdot\}$ is the operator that project each entry of a vector on the unit complex circle (i.e., entry-wise normalization). Hence, we have a majorization-minimization algorithm [11] to solve for (15) (that looks like a modified power method). The algorithm is summed up in the box Algorithm 1. Notice that this algorithm can also be used to solve the standard PL formulations, where $\mathbf{M}$ is constructed from a plug-in estimate of $\boldsymbol{\Sigma}$ [7, 5, 10].

Final algorithm

The final algorithm is shown in the box Algorithm 2 and is denoted as MLE-PL.

Algorithm 1 MM algorithm for Phase-linking problem (12)

1: **Entry:** $\mathbf{M} \in \mathbb{C}^{N \times N}$, $\mathbf{w}_0 \in \mathcal{U}_N$
2: **repeat**
3:     Compute $\tilde{\mathbf{w}}_t = (\lambda_{\max}^{\mathbf{M}}\mathbf{I} - \mathbf{M})\mathbf{w}_t$
4:     Update $\mathbf{w}_t = \mathcal{P}_{\mathcal{U}_N}\{\tilde{\mathbf{w}}_t\}$
5:     $t = t + 1$
6: **until** Convergence
7: **Output:** $\mathbf{w} \in \mathcal{U}_N$

Algorithm 2 BCD algorithm for MLE problem (7)

1: **Entry:** SCM $\mathbf{S}$
2: **repeat**
3:     Update $\boldsymbol{\Sigma}$ with (11)
4:     Call Algorithm 1 with $\mathbf{M} = \boldsymbol{\Sigma}^{-1} \circ \mathbf{S}$
5:     Update $\boldsymbol{\theta}$ from the output of Algorithm 1
6: **until** Convergence
7: **Output:** MLEs $\boldsymbol{\Sigma}$, $\boldsymbol{\theta}$ and $\mathbf{C}(\boldsymbol{\Sigma}, \boldsymbol{\theta})$

---

4. SIMULATION

To assess the performance of the proposed algorithm, we generate a matrix $\mathbf{C}$ from (4). The covariance matrix $\boldsymbol{\Sigma}$ is chosen as a Toeplitz matrix with coherence coefficient ρ ranging from 0.5 to 0.9. The N SAR phases are generated as random values in $(-\pi, \pi)$, yielding $\boldsymbol{\theta} = [-1.13, 0.25, 2.37, -1.78, -0.67]$ for all Monte-Carlo runs. At last, L i.i.d samples are then simulated from the distribution (2). A spatial window of L pixels is ranging from 6 to 100 with $N = 5$ dates and 1000 number of Monte Carlo simulations.

For comparison, other methods are also tested: 2p-InSAR is a common InSAR processing in which InSAR phases are only estimated in spatial dimension and with the use of a multilooking window. PL is the conventional 2-step phase linking [10]: $\mathbf{M} = \boldsymbol{\Sigma}^{-1} \circ \mathbf{S}$ is constructed with the plug-in estimate $\hat{\boldsymbol{\Sigma}}_{\text{mod}} = |\mathbf{S}|$ (entry-wise modulus), then problem (15) is solved to obtain the phases estimates. In our setting, we use Algorithm 1 to solve (15).

We first test the convergence of the MLE-PL method in Figure 2 for $L = 20$ and $\rho = 0.5$. The cost function related to (7) is decreasing and reaches convergence after 7 iterations. In the following part of this study, the number of iterations is set to 10 to ensure the convergence of the MLE-PL.
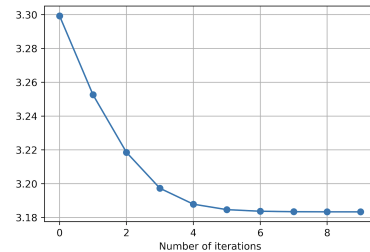
Fig. 2. Cost function of the MLE-PL method with $L = 20$, $N = 5$, $\rho = 0.5$.

For one true InSAR phase, Figure 3 shows the histogram of the estimates obtained by different methods with $N = 5$, $L = 20$ and $\rho = 0.7$. All the methods give estimated values around the simulated InSAR value. The empirical variance of the MLE-PL and the PL estimates appear lower compared to the 2p-InSAR one.
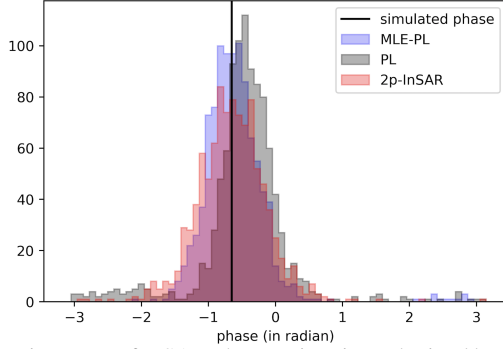

Fig. 3. Histogram of InSAR phase estimations obtained by $MLE-PL$, PL and $2p$-InSAR. $L = 20$, $N = 5$, $\rho = 0.7$.

Figure 4 presents the Mean Squared Error (MSE) of estimated InSAR phases for the different methods and in terms of the number of pixels within a spatial window of L pixels. Different values of the coherence coefficient are studied, from high coherence ($\rho = 0.9$) to medium coherence ($\rho = 0.7$) to low coherence ($\rho = 0.5$). The MSE of each method decreases with the number of available samples which is expected. Interestingly, we observe that MLE-PL allows for an improvement of the accuracy of the phase estimation compared to PL or 2p-InSAR in all the considered setups.
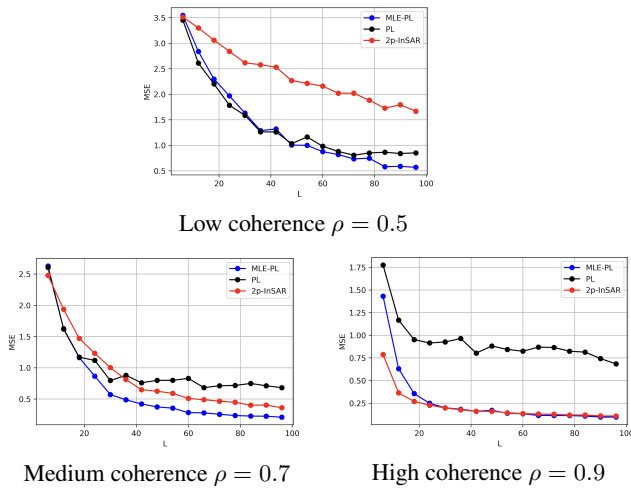

Low coherence $\rho = 0.5$

Medium coherence $\rho = 0.7$ High coherence $\rho = 0.9$

Fig. 4. MSE of InSAR estimates using 2p-InSAR, PL and MLE-PL with Gaussian distributed input data. $N = 5$, 1000 Monte Carlo trials.

5. CONCLUSION

In this paper, a new phase linking algorithm based on MLE was proposed and applied to simulated data. This MLE-PL algorithm was obtained by jointly solving the estimation of all parameters (phases and covariance matrix). Additionally, we derived a Majorization-Minimization algorithm to solve the PL step that is also suitable to others standard PL approaches. Simulations illustrated that this new method offers some improvement in terms of MSE for various degree of temporal coherence.

6. REFERENCES

[1] R. Prébet, Y. Yan, M. Jauvin, and E. Trouvé, "A data-adaptive EOF-based method for displacement signal retrieval from InSAR displacement measurement time series for decorrelating targets," IEEE Transaction on Geoscience and Remote Sensing, vol. 57, no. 8, pp. 5829–5852, 2019.

[2] D. Ho Tong Minh, R. Hanssen, and F. Rocca, "Radar interferometry: 20 years of development in time series techniques and future perspectives," Remote Sensing, vol. 12, pp. 1364, 2020.

[3] A. Ferretti, C. Prati, and F. Rocca, "Permanent scatterers in SAR interferometry," IEEE Transactions on Geoscience and Remote Sensing, vol. 39, no. 1, pp. 8–20, 2001.

[4] R. Lanari, O. Mora, M. Manunta, J.J. Mallorqui, P. Berardino, and E. Sansosti, "A small-baseline approach for investigating deformations on full-resolution differential SAR interferograms," IEEE Transactions on Geoscience and Remote Sensing, vol. 42, no. 7, pp. 1377–1386, 2004.

[5] A. Ferretti, A. Fumagalli, F. Novali, C. Prati, F. Rocca, and A. Rucci, "A New Algorithm for Processing Interferometric Data-Stacks: SqueeSAR," IEEE Transactions on Geoscience and Remote Sensing, vol. 49, no. 9, pp. 3460–3470, 2011.

[6] H. Ansari, F. De Zan, and A. Parizzi, "Study of systematic bias in measuring surface deformation with SAR interferometry," IEEE Transactions on Geoscience and Remote Sensing, vol. 59, no. 2, pp. 1285–1301, 2021.

[7] A. Monti-Guarnieri and S. Tebaldini, "On the exploitation of target statistics for SAR interferometry applications," IEEE Transactions on Geoscience and Remote Sensing, vol. 46, no. 11, pp. 3436–3443, 2008.

[8] H. Ansari, F. De Zan, and R. Bamler, "Efficient phase estimation for interferogram stacks," IEEE Transactions on Geoscience and Remote Sensing, vol. 56, no. 7, pp. 4109–4125, 2018.

[9] H. Ansari, F. De Zan, and R. Bamler, "Sequential estimator: Toward efficient InSAR time series analysis," IEEE Transactions on Geoscience and Remote Sensing, vol. 55, no. 10, pp. 5637–5652, 2017.

[10] N. Cao, H. Lee, and H. C. Jung, "Mathematical framework for phase-triangulation algorithms in distributed-scatterer interferometry," IEEE Geoscience and Remote Sensing Letters, vol. 12, no. 9, pp. 1838–1842, 2015.

[11] Y. Sun, P. Babu, and D. P. Palomar, "Majorization-minimization algorithms in signal processing, communications, and machine learning," IEEE Transactions on Signal Processing, vol. 65, no. 3, pp. 794–816, 2016.